POLISH
JOURNAL *of* RADIOLOGY

http://www.polradiol.com

Original paper

A descriptive neuroimaging study of retinoblastoma in children: magnetic resonance imaging features

Gunes Orman[A,B,C,D,E,F], Thierry A.G.M. Huisman[A,E]

Texas Children's Hospital, USA

Abstract

Purpose: Retinoblastoma (RB) is the most common intraocular malignancy of childhood. Magnetic resonance imaging (MRI) is essential for initial diagnosis, tumour extension, staging, and treatment planning of RB. Awareness of neuroimaging findings and determining local extent are essential for early diagnosis and therapy guidance. The purpose of this study is to evaluate and to provide a detailed list of neuroimaging features of RB to improve the diagnostic work-up of children with RB.

Material and methods: Retrospective review was performed among children with confirmed RB diagnosis. MRI features were identified to evaluate: 1) growth pattern; 2) intraocular extension; 3) extraocular extension; 4) central nervous system disease; 5) conventional MRI characteristics of the RB lesions; and 6) DWI and ADC characteristics. These features were compared between unilateral and bilateral RB lesions.

Results: Twenty-four children (male/female: 18/6) were included in this study. The mean age at the time of diagnosis was 14.7 (11.4) months. In total, 34 RB lesions (bilateral = 18) were evaluated for the study. The most common features on MRI were: 1) endophytic RB lesion (50%); 2) subretinal haemorrhage (38%); 3) scleral involvement (3%); 4) leptomeningeal disease (12%); 5) contrast enhancement (97%); and 6) restricted diffusion (88%). The mean ADC value was $0.64 (0.15) \times 10^{-3}$ mm²/s. Choroidal invasion ($p = 0.05$) and scleral involvement ($p = 0.04$) were significantly higher for bilateral RB lesions.

Conclusions: Contrast enhancement and restricted diffusion are the most common neuroimaging features of RB. Choroidal invasion and scleral involvement are more frequently seen in bilateral disease.

Key words: bilateral, diffusion-weighted imaging, neuroimaging, retinoblastoma, unilateral.

Introduction

Retinoblastoma (RB) is the most frequent malignant ocular tumour in children, typically presenting in the first years of life. It represents approximately 3% of all paediatric malignancies, with an incidence of 1 : 17,000 [1]. Magnetic resonance imaging (MRI) is used primarily for local tumour staging and depiction of associated intracranial primitive neuroectodermal tumours (mostly pineoblastoma). MRI is an especially important diagnostic tool for the detection of local tumour extent in ad-

vanced retinoblastoma. The most common clinical sign of RB is leukocoria (60%) followed by strabismus (20%) [2]. The treatment strategy is focused on survival, preserving vision, and avoiding enucleation. The treatment strategy is frequently based on clinical and imaging findings only. Important risk factors for local recurrence and metastasis are massive choroidal invasion, scleral invasion, and optic nerve invasion posterior to the lamina cribrosa [1]. MRI is essential for monitoring patients after treatment and for detection of associated second malignancies. A highly specific and sensitive diagnostic workup of local

invasion is important to guide treatment and preserve vision if possible. Computed tomography (CT) has been used to define tumour calcification in the past, but because of the potential increased risk of secondary cancers due to exposure to ionizing radiation, especially in germline RB, the role of CT in the evaluation of RB is now historical and has been replaced by ultrasonography or MRI [3].

Awareness of the neuroimaging findings of RB and determining local extent are mandatory for an early diagnosis and therapy guidance and, subsequently, to improve the long-term outcome. The purpose of this study is to evaluate and provide a detailed list of the imaging features using various MRI sequences with particular interest in the local extent and varying signal characteristics to improve diagnostic work-up of children with RB.

Material and methods

Following institutional review board approval, a retrospective review was performed among children (0-17 years old) with histopathologically confirmed RB diagnosis over a 10-year period with diagnostic MRI studies for this single-centre study.

All patients were imaged using the standard departmental imaging protocols including multiplanar pre- and post-contrast-enhanced T1- and T2-weighted (T1-W and T2-W) sequences as well as susceptibility-weighted imaging (SWI) and diffusion tensor imaging (DTI). The slice thickness, field-of-view, and matrix were optimized for the age and size of the patient. Imaging included dedicated orbital sequences in addition to standard whole brain coverage. All imaging was performed on 1.5T or 3T Siemens (Erlangen, Germany) MRI scanners using a multichannel head coil.

DTI was performed using a single-shot spin-echo echoplanar (EPI) axial DTI sequence. Balanced pairs of diffusion gradients were applied along 12-20 non-collinear orthogonal directions with a high b-value of 1000 s/mm^2. An additional measurement without diffusion weighting ($b = 0$ s/mm^2) was performed. For the acquisition of the DTI data, the following parameters were used: slice thickness = 2.5 mm, FOV = 240 × 240 mm, and matrix size = 192 × 192. Parallel imaging iPAT = 2 with GRAPPA (generalized auto-calibrating partial parallel acquisition

reconstruction) was used. The acquisition was repeated twice to enhance the SNR. Isotropic DTI and matching apparent diffusion coefficient (ADC) maps were calculated.

MR images were evaluated in consensus by 2 subspecialty trained paediatric neuroimagers (AP, TAGMH) for the following features: 1) growth pattern (endophytic, exophytic, mixed); 2) intraocular extension (vitreous seeding/haemorrhage, retinal detachment and subretinal seeding/haemorrhage, anterior chamber involvement, choroidal invasion); 3) extraocular extension (scleral involvement, optic nerve involvement); 4) central nervous system disease (trilateral RB, leptomeningeal disease); 5) conventional MRI imaging characteristics of the RB lesions (T1 isointense, T2 isointense, FLAIR isointense, calcification, post-contrast enhancement); and 6) DWI and ADC characteristics [3,4].

ADC values were sampled from within the lesion using a region of interest (ROI) approach. The ROIs were hand drawn on the ADC maps using the patient archiving and communication system (PACS). One ROI was drawn per lesion on the slice with apparent maximal tumour extension/size.

Statistical analysis

Statistical analysis of data was performed using SPSS version 10 (SPSS, Chicago, Illinois). Fisher's exact test was used to determine the differences between bilateral and unilateral RB lesions for each MRI feature (calcification, vitreous haemorrhage, anterior chamber involvement, optic nerve involvement, orbital disease, leptomeningeal disease, choroidal invasion, and scleral involvement). An unpaired t-test was used to compare mean ADC results between bilateral and unilateral RB lesions. The p-value was considered significant if ≤ 0.05 at the confidence interval of 95%.

Results

Twenty-four children (male/female: 18/6) were included in this study. The mean age at the time of diagnosis was 14.7 (11.4) [mean (SD)] months, (range from 3 weeks to 3 years). Sixteen children had unilateral tumours (67%), 6 children had bilateral tumours (25%), and 2 children had multiple RB lesions (8%): 1 patient had 1 tumour on the right side and 2 tumours on the left side, the other patient had 2 tumours on the right side and 1 tumour on the left side (Table 1). These lesions were counted as bilateral when evaluating MRI features. All MRI examinations reported in this study were performed prior to treatment.

In total, 34 RB lesions (19 left-sided, 15 right-sided), 18 of which were bilateral, were included in this study. MRI features were: 1) growth pattern – 50% endophytic ($n = 17$), 47% exophytic ($n = 16$), and 3% mixed ($n = 1$); 2) intraocular extension – vitreous haemorrhage was seen in 3% ($n = 1$), subretinal haemorrhage was seen in 38%

Table 1. Patient characteristics ($N = 24$)

Factor	
Sex (male), n (%)	18 (75)
Age (less than 12), n (%)	13 (54)
Age (mean, months)	14.7 (mean); 11.4 (SD)
Single tumour, n (%)	16 (67)
Double tumour, n (%)	6 (25)
Multiple tumour, n (%)	2 (8)

(n = 13), anterior chamber was involved in 21% (n = 7), and choroidal invasion was seen in 26% (n = 9) of RB lesions; 3) extraocular extension – scleral involvement was seen in 3% (n = 1) and optic nerve involvement was seen in 3% (n = 1) of RB lesions; 4) central nervous system disease – there was 0% (n = 0) trilateral RB, leptomeningeal disease was seen in 12% (n = 4) of RB lesions; 5) conventional MRI imaging characteristics – 82% T1 isointense (n = 28), 21% T2 isointense (n = 7), 50% FLAIR isointense (n = 17), calcification was seen in 35% of the lesions (n = 12), and contrast enhancement was noted in 97% of the RB lesions (n = 33); and 6) restricted diffusion was seen in 88% (n = 23) of 26 RB lesions included. The mean (SD) ADC value of the RB lesions was 0.64 (0.15) × 10⁻³ mm²/s of the 24 RB lesions included (Table 2).

No significant differences were found between bilateral and unilateral RB lesions for calcification (p = 0.15), vitreous haemorrhage (p = 0.13), anterior chamber involvement (p = 1.00), optic nerve involvement (p = 0.47), orbital disease (p = 0.47), or leptomeningeal disease (p = 0.47) by Fisher's exact test. However, choroidal invasion (p = 0.05) and scleral involvement (p = 0.04) was significantly more frequent in bilateral RB lesions by Fisher's exact test. No significant difference was found for ADC values comparing bilateral RB lesions [0.68 (0.15) × 10⁻³ mm²/s] and unilateral RB lesions [0.63 (0.16) × 10⁻³ mm²/s] by unpaired t-test (p = 0.48).

Representative cases of the tumour MRI characteristics and extension patterns are shown in Figures 1-5.

Discussion

RB is the most common primary intraocular malignancy in children. Timely diagnosis is very important to preserve the survival, eye globe, and vision of these children [3]. Neuroimaging is an essential part for the initial diagnosis, as well as staging and treatment planning of the RB. Typical MRI findings of RB include slightly higher signal intensity than ocular fluid on T1-weighted images and low signal intensity on T2-weighted images, with contrast enhancement and restricted diffusion [4].

In this study we evaluated the MRI findings of 24 children with 34 RB lesions (18 bilateral). We found 50% of the lesions to be endophytic. Anterior chamber involvement was noted in 21% and choroidal invasion was seen in 26% of all RB lesions in our series. Galluzzi *et al.* reported 14/34 affected eyes to show abnormal gadolinium enhancement in the anterior chamber, and histopathologic evidence of optic nerve and/or choroid infiltration correlated significantly with abnormal enhancement [5]. De Graaf *et al.* found 66% sensitivity and 96% specificity for anterior chamber hyperintensity [6]. De Graaf *et al.* reported choroidal invasion with MRI in 21 eyes with 73% sensitivity and 72% specificity [6]. Exophytic growth can result in tumour invasion of the choroid. MRI findings

Table 2. Tumour characteristics (*N* = 34 lesions)

Factor	*n* (%)
Growth pattern	
Endophytic	17 (50)
Exophytic	16 (47)
Mixed	1 (3)
Intraocular extension	
Vitreous seeding/haemorrhage	1 (3)
Subretinal seeding/haemorrhage	13 (38)
Anterior chamber involvement	7 (21)
Choroidal invasion	9 (26)
Extraocular extension	
Scleral involvement	1 (3)
Optic nerve involvement	1 (3)
Central nervous system disease	
Leptomeningeal disease	4 (12)
No pineal lesions²	33 (100)
Conventional MRI characteristics	
T1 (isointense vs. hypointense)	28 (82)
T2 (isointense vs. hypointense)	7 (21)
FLAIR (isointense vs. hypointense)	17 (50)
Calcification	12 (35)
Enhancement	33 (97)
DWI-ADC characteristics	
DWI (restricted versus normal)¹	23 (88)
ADC value³	0.64 (mean); 0.15 (SD)

ADC – apparent diffusion coefficient, DWI – diffusion-weighted imaging, FLAIR – fluid-attenuated inversion recovery
¹26 included, ²33 included, ³24 included

include choroidal thickening, either enhancing or non-enhancing, or a focal region of choroidal thinning with decreased enhancement [6,7]. Kaliki *et al.* reported the histopathologic high-risk features in their patient group, including anterior chamber seeding (17%), iris infiltration (8%), ciliary body infiltration (12%), massive tumour size (> 3 mm), choroidal invasion (48%), post-laminar optic nerve invasion (49%), invasion of optic nerve (2%), combined choroid and optic nerve invasion (12%), scleral infiltration (14%), and extrascleral involvement (6%) [8]. In our study we found choroidal invasion (p = 0.05) and scleral involvement (p = 0.04) to be present significantly more frequently in cases of bilateral RB lesions.

Restricted diffusion was seen in 88% of our patients, which is best explained by the high/dense cellularity of the RBs. The mean ADC value was 0.64 ± 0.15 × 10⁻³ mm²/s and did not show significant differences comparing cases with unilateral versus bilateral RB lesions. Abdel Razek *et al.* reported a mean ADC value of 0.49 ± 0.12 × 10⁻³ mm²/s, which is lower than our finding. Also, they reported a sig-
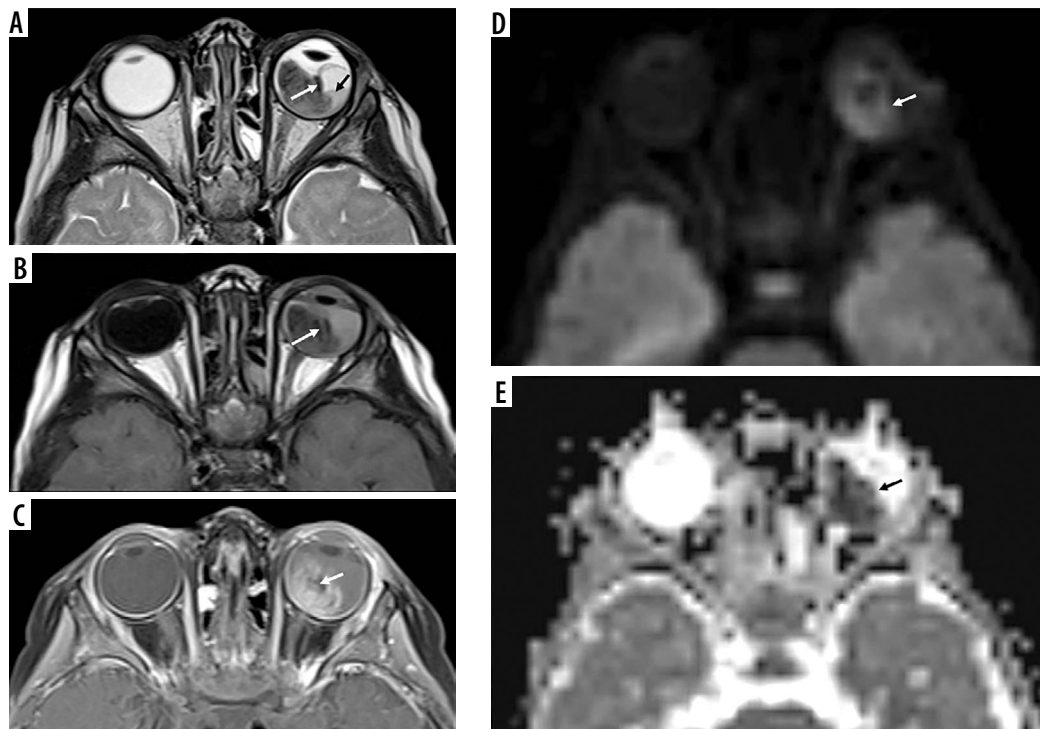
Figure 1. Unilateral retinoblastoma of the left eye. Note the left globe is slightly larger than the right globe. Axial T2 (**A**), and T1-weighted imaging (**B**) shows the heterogeneous iso/hypointense intraocular tumour on the left side involving both nasal and temporal sides. The tumour causes retinal detachment and haemorrhage with layering (**A**, black arrow). There is hypointense punctate calcification of the tumour (**A, B**, white arrow). Axial post-contrast T1-weighted imaging shows the heterogeneous enhancement, note the hypointense calcification is spared (**C**, white arrow) after contrast administration. Diffusion tensor imaging (**D**, white arrow) and apparent diffusion coefficient (**E**, black arrow) show the restricted diffusion, which is a sign of high tumour cellularity
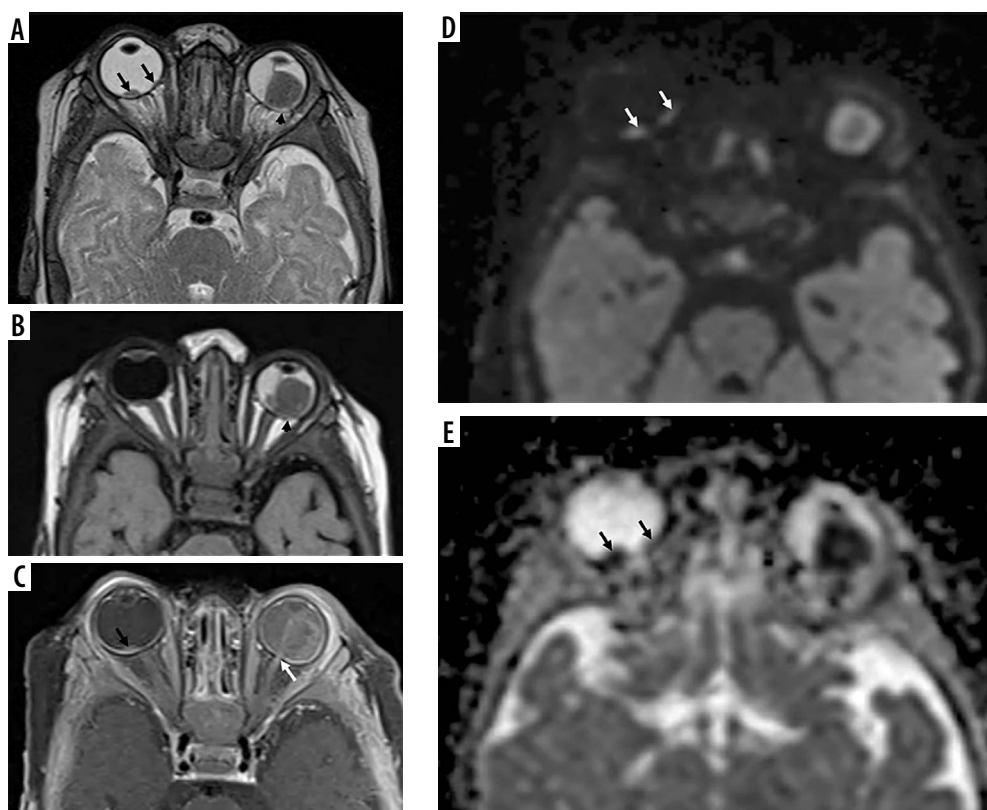

Figure 2. Bilateral multifocal retinoblastoma. Two small endophytic lesions are appreciated on the right side on the axial T2-weighted imaging (**A**, black arrows). The tiny, subtle lesion on the nasal side could be easily overlooked on the axial T1-weighted (**B**) and post-contrast T1-weighted imaging (**C**). However, diffusion tensor imaging (**D**, white arrows) and apparent diffusion coefficient (**E**, black arrows) show the lesion in a very conspicuous fashion due to the restricted diffusion of 2 distinct lesions clearly and confirm the diagnosis. The lesion on the left side involves almost half of the globe on the temporal side causing retinal detachment and haemorrhage, with signs of scleral invasion (**A, B**, black arrow) and optic disc invasion with contrast enhancement (**C**, white arrow). Restricted diffusion is much better appreciated on the left-sided large lesion (**D, E**). Note the smaller size of the globe on the left side
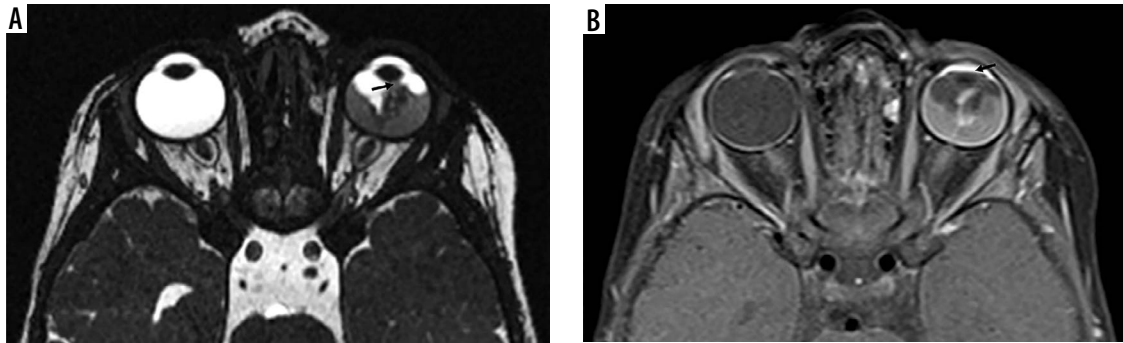
Figure 3. Unilateral retinoblastoma of the left eye. The heterogeneous isointense lesion is endophytic, involving more than half of the globe on both nasal and temporal sides extending to the iris (**A,** black arrow). Post-contrast imaging shows diffuse enhancement of the lesion with avid anterior chamber enhancement (**B,** black arrow)
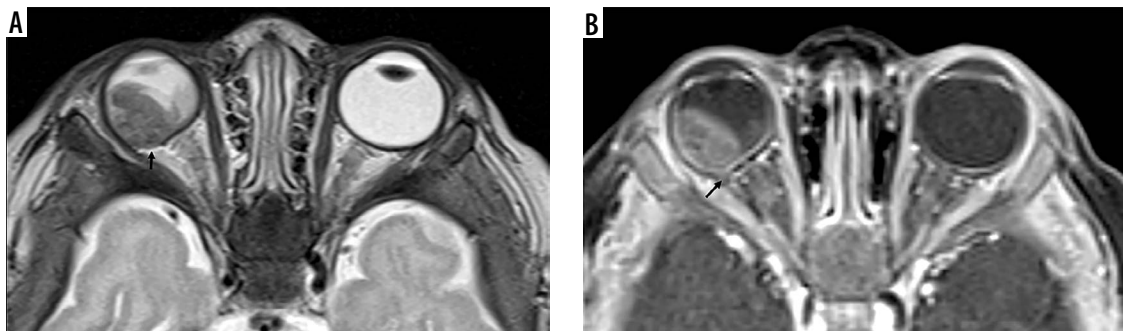

Figure 4. Unilateral retinoblastoma of the right eye. The heterogeneous hypointense lesion involving mostly on the temporal side causing scleral involvement (**A, B,** black arrow)
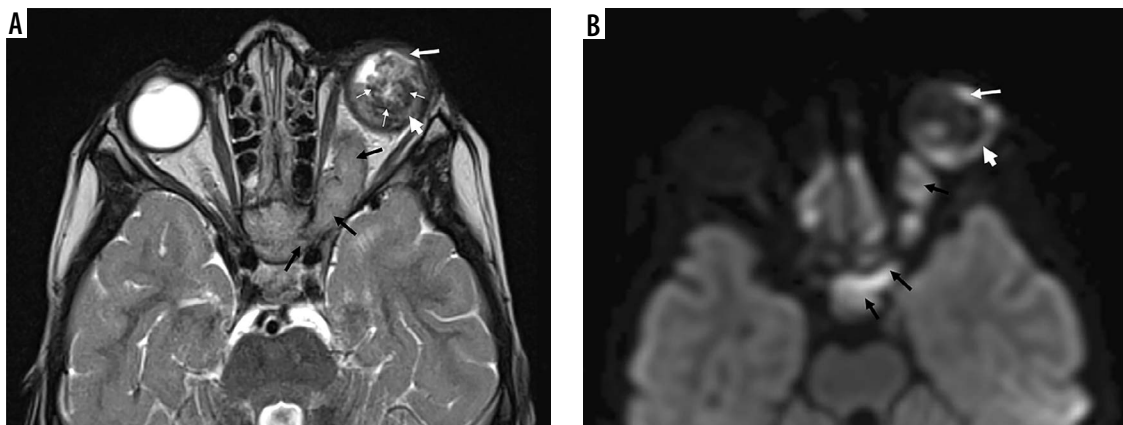

Figure 5. Unilateral retinoblastoma of the left eye with extensive involvement. Axial T2-weighted imaging and diffusion tensor imaging show an isointense heterogeneous lesion with gross hypointense calcifications (**A,** thin white arrows), with scleral involvement (**A, B,** arrowhead), extending to the anterior chamber (**A, B,** thick white arrow), and to the left optic nerve and optic chiasm (**A, B,** black arrows)

nificantly lower mean ADC value in bilateral RB lesions compared to unilateral RB lesions [9]. Sepahdari *et al.* reported a mean ADC value of $0.93 \pm 0.3 \times 10^{-3}$ mm²/s in 15 RBs in their study of DWI of malign ocular tumours, and the ADC of RB was inversely correlated with lesion thickness. They concluded that this finding represented the effect of partial volume averaging [10]. De Graaf *et al.* reported significantly different mean ADC values between enhancing (1.03 [0.72-1.22] $\times 10^{-3}$ mm²/s) and non-enhancing (1.47 [0.99 –1.80] $\times 10^{-3}$ mm²/s) parts of RB lesions [11]. Hiwatashi *et al.* compared ADC measurements of RB

lesions between diffusion-sensitized driven-equilibrium turbo field echo (DSDE-TFE) and echoplanar (EP) diffusion weighted imaging. On the DSDE-TFE, the mean ADC value was $1.73 \pm 0.73 \times 10^{-3}$ mm²/s. On the EP images, the mean ADC value was $0.93 \pm 0.53 \times 10^{-3}$ mm²/s with significant correlation between DSDE-TFE and EP images [12]. The variety in mean ADC values in these studies may be because of: 1) different tumour cellularity/stage in different study patient groups; 2) subjective measurement methods; or 3) different technical parameters using different MRI devices for the different studies.

Limitations in this study are: 1) retrospective nature of the study; 2) single-centre evaluation; and 3) no genetic sampling was performed to exclude inherited retinoblastoma.

Conclusions

The most common features of paediatric RB on MRI are: 1) endophytic RB lesion (50%); 2) subretinal haemorrhage (38%); 3) scleral involvement (3%); 4) leptomeningeal disease (12%); 5) contrast enhancement (97%); and 6) restricted diffusion (88%). The mean ADC value was $0.64 \pm 0.15 \times 10^{-3}$ mm^2/s. Bilateral RB lesions show higher frequency of choroidal invasion and scleral involvement compared to unilateral RB lesions. Certain MRI characteristics may be helpful to differentiate unilateral and bilateral RB lesions; however, our study did not reveal significantly different ADC values comparing patients with unilateral versus bilateral presentations.

Acknowledgements

We would like to thank Dr. Andrea Poretti for his contribution during the initial design phase of this project.

Conflicts of interest

The authors report no conflict of interest.

References

1. de Jong MC, de Graaf P, Noij DP, et al. Diagnostic performance of magnetic resonance imaging and computed tomography for advanced retinoblastoma: a systematic review and meta-analysis. Ophthalmology 2014; 121: 1109-1118.

2. Razek AA, Elkhamary S. MRI of retinoblastoma. Br J Radiol 2011; 84: 775-784.

3. Silvera VM, Guerin JB, Brinjikji W, et al. Retinoblastoma: what the neuroradiologist needs to know. AJNR Am J Neuroradiol 2021; 42: 618-626.

4. Rauschecker AM, Patel CV, Yeom KW, et al. High-resolution MR imaging of the orbit in patients with retinoblastoma. Radiographics 2012; 32: 1307-1326.

5. Galluzzi P, Cerase A, Hadjistilianou T, et al. Retinoblastoma: abnormal gadolinium enhancement of anterior segment of eyes at MR imaging with clinical and histopathologic correlation. Radiology 2003; 228: 683-690.

6. de Graaf P, Barkhof F, Moll AC, et al. Retinoblastoma: MR imaging parameters in detection of tumor extent. Radiology 2005; 235: 197-207.

7. Sirin S, de Jong MC, de Graaf P, et al. High-resolution magnetic resonance imaging can reliably detect orbital tumor recurrence after enucleation in children with retinoblastoma. Ophthalmology 2016; 123: 635-645.

8. Kaliki S, Srinivasan V, Gupta A, et al. Clinical features predictive of high-risk retinoblastoma in 403 Asian Indian patients: a case-control study. Ophthalmology 2015; 122: 1165-1172.

9. Abdel Razek AA, Elkhamary S, Al-Mesfer S, et al. Correlation of apparent diffusion coefficient at 3T with prognostic parameters of retinoblastoma. AJNR Am J Neuroradiol 2012; 33: 944-948.

10. Sepahdari AR, Kapur R, Aakalu VK, et al. Diffusion-weighted imaging of malignant ocular masses: initial results and directions for further study. AJNR Am J Neuroradiol 2012; 33: 314-319.

11. de Graaf P, Pouwels PJ, Rodjan F, et al. Single-shot turbo spin-echo diffusion-weighted imaging for retinoblastoma: initial experience. AJNR Am J Neuroradiol 2012; 33: 110-118.

12. Hiwatashi A, Togao O, Yamashita K, et al. 3D turbo field echo with diffusion-sensitized driven-equilibrium preparation technique (DSDE-TFE) versus echo planar imaging in evaluation of diffusivity of retinoblastoma. Br J Radiol 2016; 89: 20160074.